Inorganic Chemistry

including bioinorganic chemistry

October 20, 2014
Volume 53, Number 20
pubs.acs.org/IC

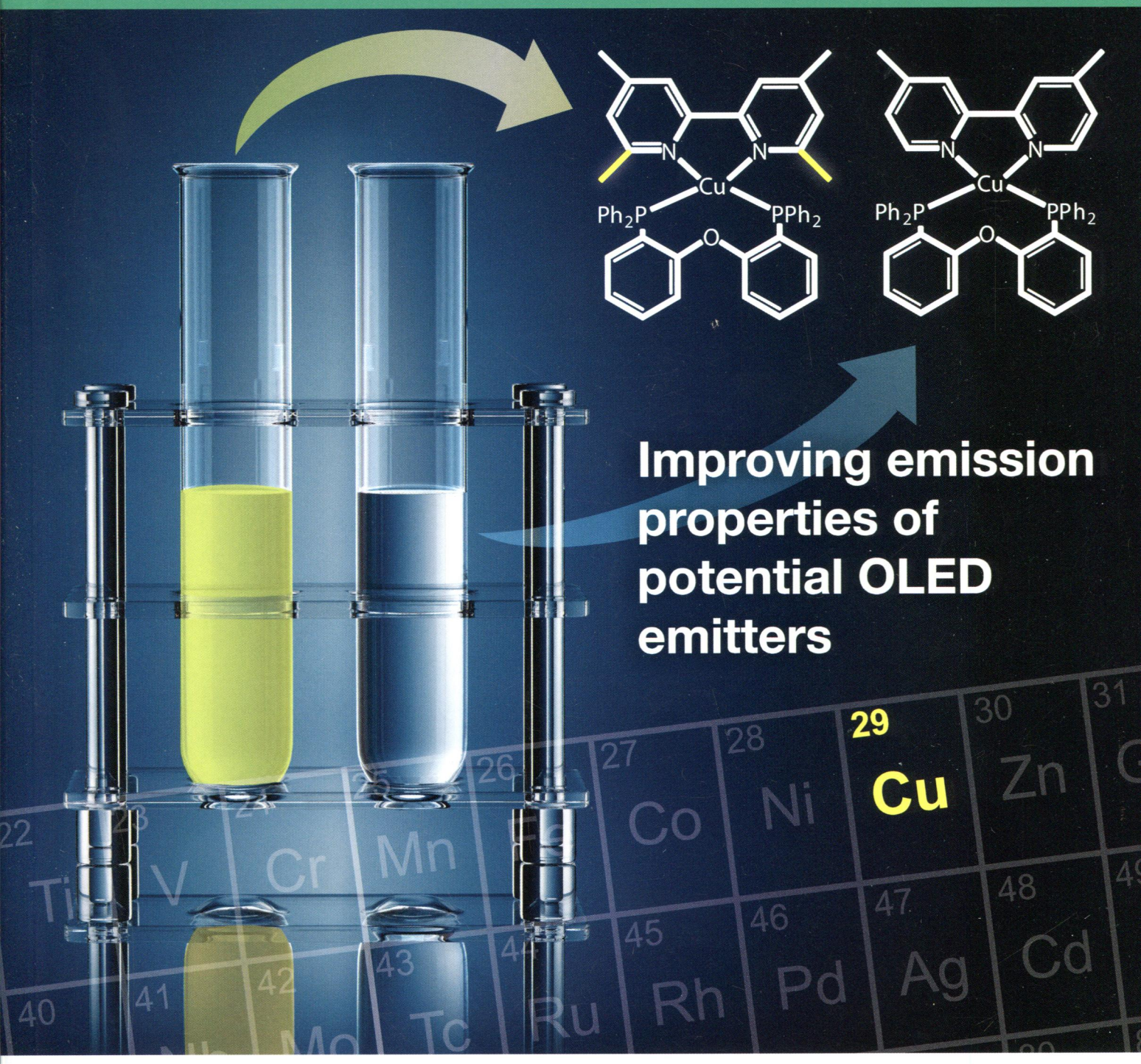

ACS Publications
Most Trusted. Most Cited. Most Read.

www.acs.org

Inorganic Chemistry

OCTOBER 20, 2014
VOLUME 53 ISSUE 20

INOCAJ 53(20) 10781–11344 (2014)
ISSN 0020-1669
Registered in the U.S. Patent and Trademark Office

ON THE COVER: Cu(I) compounds exhibiting a thermally activated delayed fluorescence (TADF) are highly attractive for use as emitters in organic light-emitting diodes (OLEDs). However, this class of complexes distorts significantly on excitation. As a consequence, strong nonradiative deactivation and thus photoluminescence quenching occur. With the introduction of sterically demanding groups (methyl groups marked in yellow), these distortions can be minimized and the emission quantum yield can be significantly increased. Cover design by Iris Profendiner. See C. L. Linfoot, M. J. Leitl, P. Richardson, A. F. Rausch, O. Chepelin, F. J. White, H. Yersin, and N. Robertson, p 10854.

Editorial

Communications

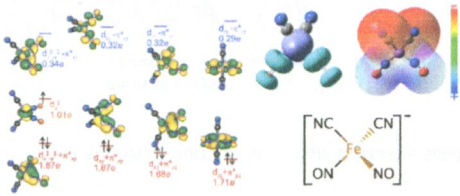

10788 dx.doi.org/10.1021/ic5011743

Synthesis and Dynamic Behavior of an Anthyridine-Ligated Ruthenium Complex

Shota Hirakawa and Take-aki Koizumi*

A new ruthenium complex, $[\mathbf{1}](PF_6)_2$, containing a 1,9,10-anthyridine derivative (L) was synthesized, and its dynamic behavior was investigated. L in $[\mathbf{1}](PF_6)_2$ is coordinated to the Ru center as a bidentate ligand. When $[\mathbf{1}](PF_6)_2$ was dissolved in acetonitrile, a new complex incorporating one acetonitrile molecule, $[\mathbf{2}](PF_6)_2$, was formed. In $[\mathbf{2}](PF_6)_2$, L is coordinated to the Ru center in a monodentate fashion. The coordinated L in $[\mathbf{2}](PF_6)_2$ shows a unique haptotropic rearrangement in a CH_3CN solution.

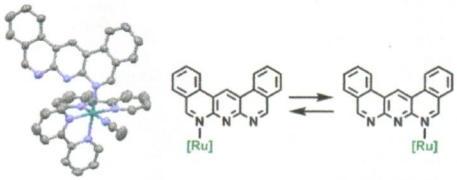

10791 dx.doi.org/10.1021/ic5013186

Visual Synchronous Exchange of Metal Nodes and Counteranions Constituting a Cobalt(II) Coordination Polymer

Jian-Cheng Wang, Qi-Kui Liu, Jian-Ping Ma, Fang Huang, and Yu-Bin Dong*

A visual simultaneous exchange of metal nodes and counteranions based on a 1D cobalt(2+) coordination polymer is reported.

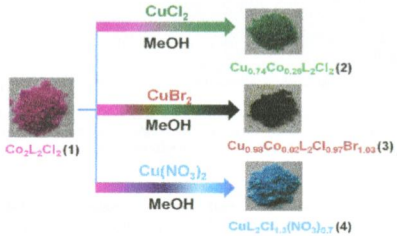

10794 dx.doi.org/10.1021/ic501496a

Strongest Exchange Coupling in Gadolinium(III) and Nitroxide Coordination Compounds

Takuya Kanetomo and Takayuki Ishida*

The largest antiferromagnetic coupling parameter was characterized to be $2J/k_B = -15.9(2)$ K in $[Gd(hfac)_3(6bpyNO)]$, where 6bpyNO stands for 2,2′-bipyridin-6-yl-*tert*-butyl nitroxide. This molecule was designed according to the empirical relation: more planar chelate favors stronger antiferromagnetic coupling. The $Gd-O_{6bpyNO}$ bond is relatively short owing to the tridentate character.

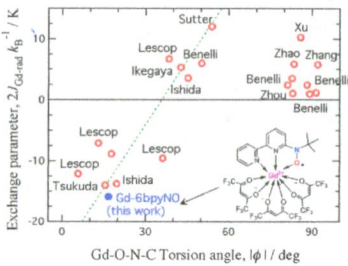

10797 S dx.doi.org/10.1021/ic501598h

Formation of Self-Assembled Defect-Free Zn_2SnO_4 Nanostructures from Binary Oxides without the Kirkendall Effect
Partha Pratim Das and Parukuttyamma Sujatha Devi*

We report here a facile approach to synthesizing a technologically important oxide Zn_2SnO_4 (ZTO) by a temperature-dependent solid-state reaction occurring without any Kirkendall effect. ZTO prepared by this single-step process could be projected as an efficient photocatalyst for wastewater treatment and a potential photoanode for dye-sensitized solar cell applications.

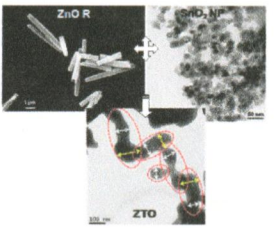

10800 S dx.doi.org/10.1021/ic502003j

Simultaneous Presence of Two Different Magnetic Structures in a Single-Crystalline Solid? Hydrogen-Distribution-Dependent Magnetism
Hyun-Joo Koo* and Myung-Hwan Whangbo*

The explanation for the neutron diffraction patterns of a crystalline solid, $NaFe_2(H_3O_2)(MoO_4)_2$, requires the assumption that two different magnetic structures coexist simultaneously. The cause for this observation was examined.

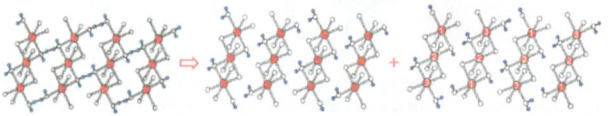

Articles

10803 S dx.doi.org/10.1021/ic5002545

The Structural Conversion of Multinuclear Titanium(IV) μ-Oxo-complexes
Aleksandra Radtke, Piotr Piszczek,* Tadeusz Muzioł, and Andrzej Wojtczak

The crystallographic and spectral studies revealed the conversion of $[Ti_6O_6(O^tBu)(O_2CR')_6]$ clusters into $[Ti_4O_4(O^tBu)_4(O_2CR')_4]$, which proceeds with the formation of the intermediate system.

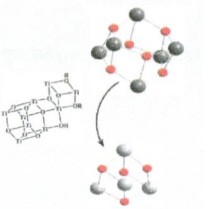

10811 dx.doi.org/10.1021/ic500454d

Molecular Structures and Solvation of Free Monomeric and Dimeric Ferriheme in Aqueous Solution: Insights from Molecular Dynamics Simulations and Extended X-ray Absorption Fine Structure Spectroscopy

David Kuter, Victor Streltsov, Natalia Davydova, Gerhard A. Venter, Kevin J. Naidoo,* and Timothy J. Egan*

Force field parametrization and molecular dynamics simulation of monomeric and dimeric ferriheme species in aqueous solution were conducted using CHARMM. The structure and solvation of simulated ferriheme species were investigated. EXAFS spectra of solid and frozen solution of μ-oxo ferriheme were consistent with crystallographic and computed data, respectively. The newly developed model successfully simulated five-coordinate ferriheme species in non-protein-bound, aqueous solution.

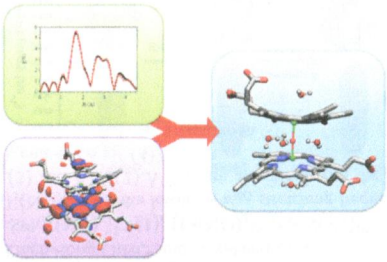

10825 dx.doi.org/10.1021/ic500683f

Encapsulation of the 4-Mercaptobenzoate Ligand by Macrocyclic Metal Complexes: Conversion of a Metallocavitand to a Metalloligand

Jochen Lach, Alexander Jeremies, Daniel Breite, Bernd Abel, Benjamin Mahns, Martin Knupfer, Vitaly Matulis, Oleg A. Ivashkevich, and Berthold Kersting*

The macrocyclic complex $[Ni_2L(\mu\text{-}Cl)]^+$ reacts selectively with the carboxylate function of the ambidentate ligand 4-mercaptobenzoate to produce the carboxylato-bridged complex $[Ni_2L(\mu\text{-}O_2C_6H_4SH)]^+$. The reactivity of this species is reminiscent of that of a pure thiolate ligand, with the exposed thiol group being (a) reversibly oxidized to the disulfide $[\{Ni_2L\}_2(O_2C_6H_4S)_2]^{2+}$, (b) aurated with $[AuCl(PPh_3)]$ to form trinuclear $[Ni_2L(O_2CC_6H_4S)AuPPh_3]^+$, or (c) chemisorbed on gold. The bridging thiolate functions of the N_6S_2 macrocycle are deeply buried and shielded such that they remain unaffected under these reaction conditions.

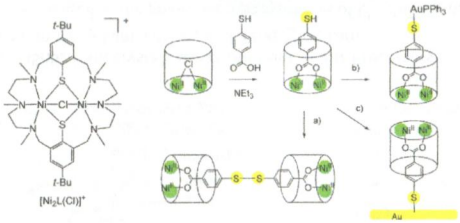

10835 dx.doi.org/10.1021/ic500772f

Magnetic Anisotropy and Mechanism of Magnetic Relaxation in Er(III) Single-Ion Magnets

Saurabh Kumar Singh, Tulika Gupta, and Gopalan Rajaraman*

In the present work, we have examined the origin of magnetic anisotropy and mechanism of magnetic relaxation in Er(III) SMMs using state-of-the-art *ab initio* calculations. Our studies on real and model complexes highlight the importance of a high symmetry environment to build large magnetic anisotropy in these complexes.

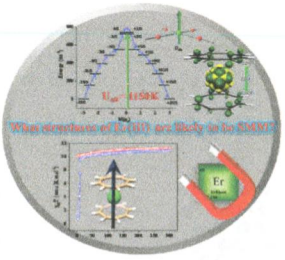

10846 dx.doi.org/10.1021/ic500816z

Quantum Chemistry Study of Uranium(VI), Neptunium(V), and Plutonium(IV,VI) Complexes with Preorganized Tetradentate Phenanthrolineamide Ligands

Cheng-Liang Xiao, Qun-Yan Wu, Cong-Zhi Wang, Yu-Liang Zhao, Zhi-Fang Chai,* and Wei-Qun Shi*

Density functional theory coupled with the quasi-relativistic small-core pseudopotential method was used to investigate the structures, bonding nature, and thermodynamic behavior of uranium(VI), neptunium(V), and plutonium(IV,VI) with phenanthrolineamides. From the viewpoint of energy, the phenanthrolineamides extract actinides in the order of $Pu^{IV} > U^{VI} > Pu^{VI} > Np^{V}$. Additionally, substitution of one ethyl group with one tolyl group in phenanthrolineamides can enhance the complexation abilities toward actinide cations.

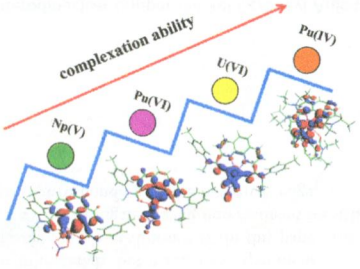

10854 dx.doi.org/10.1021/ic500889s

Thermally Activated Delayed Fluorescence (TADF) and Enhancing Photoluminescence Quantum Yields of [Cu^{I}(diimine)(diphosphine)]$^{+}$ Complexes—Photophysical, Structural, and Computational Studies

Charlotte L. Linfoot, Markus J. Leitl, Patricia Richardson, Andreas F. Rausch, Oleg Chepelin, Fraser J. White, Hartmut Yersin,* and Neil Robertson*

[Cu(I)(POP)(tmbpy)][BF_4] (**2**) shows a PLQY of 74% as a powder and also shows thermally activated delayed fluorescence, making the compound of potential application as an OLED emitter. The PLQY for [Cu(I)(POP)(dmbpy)][BF_4] (**1**), which lacks 6,6′-methyl groups on the bipy, is an order of magnitude lower. DFT calculations show that a greater torsion is possible between the ligands of **1** compared with the more constrained **2**.

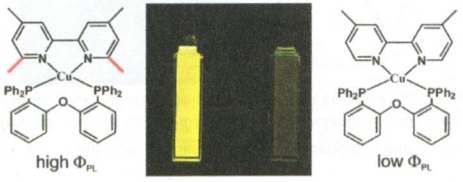

10862 S dx.doi.org/10.1021/ic500917s

Rhenium and Technetium Tricarbonyl Complexes of N-Heterocyclic Carbene Ligands

Chung Ying Chan, Paul A. Pellegrini, Ivan Greguric, and Peter J. Barnard*

A strategy for the conjugation of carboxylic acid functionalized azolium salts to biomolecules using the common peptide coupling reagent 1-ethyl-3-(3-(dimethylamino)propyl)carbodiimide is described. From these azolium salts a family of Re(I) complexes was synthesized, and for the first time an NHC ligand was radiolabeled with the medically important metallic radioisotope technetium-99m.

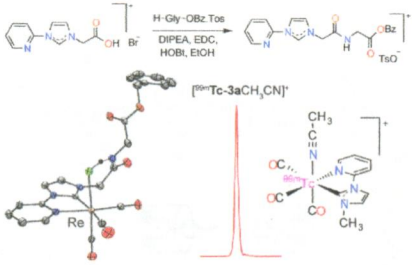

10874 S dx.doi.org/10.1021/ic500956n

Phase-Selective Synthesis of Cu_2ZnSnS_4 Nanocrystals using Different Sulfur Precursors

Zhenggang Li, Alvic Lim Kar Lui, Kwan Hang Lam, Lifei Xi, and Yeng Ming Lam*

Three sulfur-containing precursors were used in the phase-selective syntheses of Cu_2ZnSnS_4 nanocrystals. As a result, kesterite, wurtzite and mixed kesterite-wurtzite phases can be obtained due to the different rates of reaction.

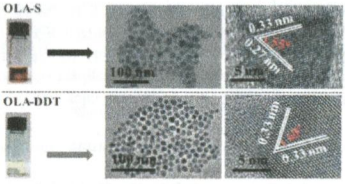

10881 S dx.doi.org/10.1021/ic501055w

Insight into the Reactivity and Electronic Structure of Dinuclear Dinitrosyl Iron Complexes

Feng-Chun Lo, Ya-Wen Li, I-Jui Hsu,* Chien-Hong Chen,* and Wen-Feng Liaw

In $\{Fe(NO)_2\}^{10}$-$\{Fe(NO)_2\}^{10}$ $[Fe_2(\mu\text{-}SPh)_2(NO)_4]^{2-}$ (**1**), $\{Fe(NO)_2\}^{9}$-$\{Fe(NO)_2\}^{10}$ $[Fe_2(\mu\text{-}SPh)_2(NO)_4]^{-}$ (**3**), and $\{Fe(NO)_2\}^{9}$-$\{Fe(NO)_2\}^{9}$ $[Fe_2(\mu\text{-}SPh)_2(NO)_4]$ (**4**), the lower IR ν_{NO} stretching frequencies and the longer N–O bond lengths (1.207(2) Å (**1**), 1.184(5) Å (**3**) and 1.165(2) Å (**4**)) are associated with the lower transition energy of $N_{1s} \rightarrow \sigma^*(NO)$ (412.2 eV (**1**), 412.3 eV (**3**), and 412.6 eV (**4**)).

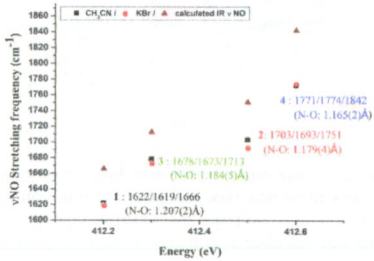

10893 S dx.doi.org/10.1021/ic501039n

H-bonded adducts of [2,4,6-{$(C_{10}H_{21}O)_3C_6H_2NH$}$_3C_3N_3$] with [LnM{$PPh_2(C_6H_4CO_2H)$}] displaying Columnar Mesophases at Room Temperature

Ana B. Miguel-Coello, Manuel Bardají,* Silverio Coco,* Bertrand Donnio, Benoît Heinrich, and Pablo Espinet*

Gold(I) or chromium(0) phosphine complexes with 4-diphenylphosphinobenzoic acid react with 2,4,6-triarylamino-1,3,5-triazine affording H-bonded supramolecular adducts displaying hexagonal columnar (Col_{hex}) mesophases.

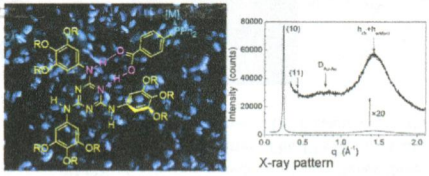

10903 dx.doi.org/10.1021/ic501730q

Detecting Non-bridging Oxygens: Non-Resonant Inelastic X-ray Scattering in Crystalline Lithium Borates

Gérald Lelong,* Guillaume Radtke, Laurent Cormier, Hanane Bricha, Jean-Pascal Rueff, James M. Ablett, Delphine Cabaret, Frédéric Gélébart, and Abhay Shukla

Probing the local environment of low-Z elements, such as oxygen, is of great interest for understanding the atomic-scale behavior in materials, but it requires experimental techniques allowing it to work with versatile sample environments. In this paper, the local environment of lithium borate crystals is investigated using non-resonant inelastic X-ray scattering (NRIXS) at energy losses corresponding to the oxygen K-edge.

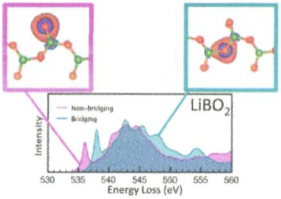

10909 S dx.doi.org/10.1021/ic501070u

Structural Evolution of Homoleptic Heterodinuclear Copper–Nickel Carbonyl Anions Revealed Using Photoelectron Velocity-Map Imaging

Zhiling Liu, Hua Xie, Zhengbo Qin, Hongjun Fan, and Zichao Tang*

Homoleptic heterodinuclear copper–nickel carbonyl anions $CuNi(CO)_n^-$ produced in the gas phase are studied using velocity-map imaging spectroscopy. The photoelectron spectra and angular distribution behaviors, complemented by computational chemistry, establish the geometrical and electronic structures of these complexes. The CO molecule is preferentially attached to the nickel atom so that the CO ligands are bonded unsymmetrically to the Ni–Cu unit, and the crossover point of the adsorption site occurs at $n = 4$.

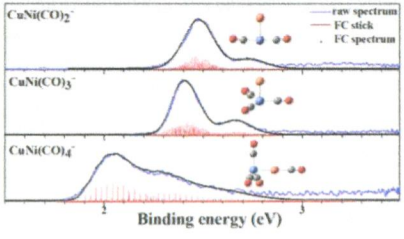

10917 dx.doi.org/10.1021/ic501121t

Multifunctional SiO_2@Gd_2O_3:Yb/Tm Hollow Capsules: Controllable Synthesis and Drug Release Properties

Guixin Yang, Ruichan Lv, Shili Gai, Yunlu Dai, Fei He, and Piaoping Yang*

Well-dispersed SiO_2@Gd_2O_3:Yb/Tm capsules with mesoporous and up-conversion luminescent properties were prepared by coating a Gd_2O_3:Yb/Tm layer on hollow mesoporous silica capsules. The size, morphology, and textural properties can be finely tuned by adjusting the cores. The composites exhibited a sustained release property and released in a pH-sensitive manner. The UC emission intensity increases with the released drug molecules, making it possible to be tracked and monitored by the change of UC luminescence simultaneously.

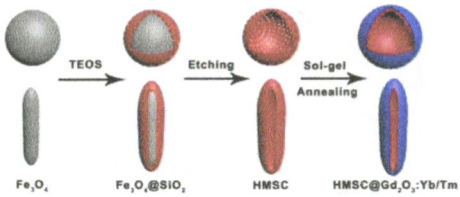

10928 S dx.doi.org/10.1021/ic501157e

Molecular Co(II) and Co(III) Heteroarylalkenolates as Efficient Precursors for Chemical Vapor Deposition of Co_3O_4 Nanowires

Mehtap Büyükyazi, Corinna Hegemann, Thomas Lehnen, Wieland Tyrra, and Sanjay Mathur*

New cobalt precursors containing Co(II) and Co(III) centers were synthesized and structurally characterized using a redox active ligand system. Both compounds are efficient precursors for catalyst-free growth of individual and hyperbranched Co_3O_4 nanowires on Si and Al_2O_3 substrates as demonstrated in a chemical vapor deposition process.

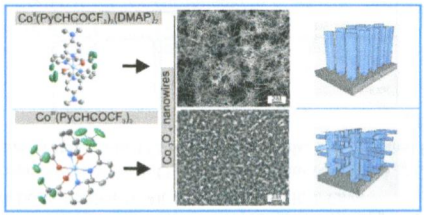

10937 S dx.doi.org/10.1021/ic501180g

Hydrothermal Synthesis of Single-Crystalline Perovskite $PbTiO_3$ Nanosheets with Dominant (001) Facets

Shiqi Deng, Gang Xu,* Huiwen Bai, Lingling Li, Shan Jiang, Ge Shen, and Gaorong Han

Single-crystalline ultrathin tetragonal perovskite $PbTiO_3$ nanosheets with dominant (001) facets were successfully synthesized via a conventional hydrothermal route by employing the layered $K_2Ti_6O_{13}$ nanofibers as titanium sources. The nanosheets are wide-band-gap semiconductors with a band gap of about 2.84 eV and exhibit strong photoluminescence emission in the visible range at room temperature.

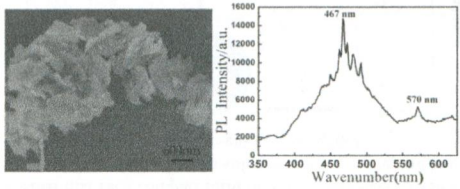

10944 S dx.doi.org/10.1021/ic5012204

Luminescent Dinuclear Cu(I) Complexes Containing Rigid Tetraphosphine Ligands

Claudia Bizzarri, Christof Strabler, Johannes Prock, Barbara Trettenbrein, Martin Ruggenthaler, Cheng-Han Yang, Federico Polo, Adriana Iordache, Peter Brüggeller,* and Luisa De Cola*

A rigid bis(bidentate) tetraphosphine was employed as bridging ligand to form homodimetallic Cu(I) species possessing interesting photophysical properties. Steric hindrance together with delayed fluorescence resulted in an intense emission (emission quantum yield of 49%) at ambient temperature in solution. We have fabricated and studied electro-luminescent devices using the related singlet emission.

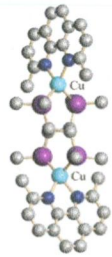

10952 S dx.doi.org/10.1021/ic501253c

Eu-MOFs with 2-(4-Carboxyphenyl)imidazo[4,5-*f*]-1,10-phenanthroline and Ditopic Carboxylates as Coligands: Synthesis, Structure, High Thermostability, and Luminescence Properties

Sheng Zhang, Yang Yang, Zheng-Qiang Xia, Xiang-Yu Liu, Qi Yang, Qing Wei, Gang Xie, San-Ping Chen,* and Sheng-Li Gao

Hydrothermal reactions of europium(III) salts with 2-(4-carboxyphenyl)imidazo[4,5-*f*]-1,10-phenanthroline and dicarboxylic acid as coligands—benzene-1,4-dicarboxylic acid, 4,4′-biphenyldicarboxylic acid, 2,5-dibromoterephthalic acid, and naphthalene-1,4-dicarboxylic acid—lead to four europium fluorescent materials (**1**−**4**). Structural analyses reveal that **1**−**4** have binuclear 3D metal−organic frameworks with different channels, void volumes, and conjugated structures tuned by ditopic carboxylates.

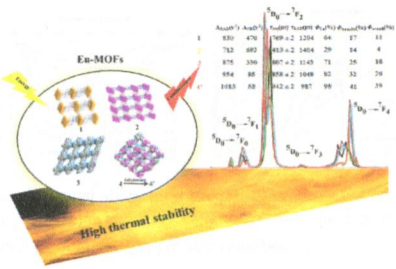

10964 S dx.doi.org/10.1021/ic501325j

Determining the Electron-Donating Properties of Bidentate Ligands by ^{13}C NMR Spectroscopy

Qiaoqiao Teng and Han Vinh Huynh*

The net donating ability of 15 bidentate ligands including aromatic and aliphatic diimines as well as alkyl-bridged di-*N*-heterocyclic carbenes was determined using a ^{13}C NMR-based electronic parameter. Differences in the substituents and the backbones affect the donating ability of the bidentate ligands according to their inductive and mesomeric effects. The methodology allows for the evaluation of classical Werner-type and organometallic ligands on a unified scale.

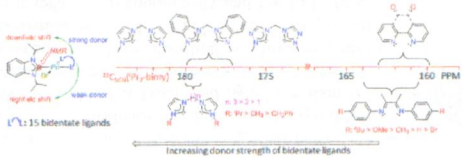

10974 dx.doi.org/10.1021/ic501351a

Synthesis, Characterization, and Spectroscopic Investigation of New Iron(III) and Copper(II) Complexes of a Carboxylate Rich Ligand and Their Interaction with Carbohydrates in Aqueous Solution

Christopher D. Stewart, Hadi Arman, Huda Bawazir, and Ghezai T. Musie*

Novel water-soluble *tetra*-iron(III) and *di*-Cu(II) complexes exhibiting strong carbohydrate interaction were synthesized. Stabilities and interaction of the complexes toward biologically relevant monosaccharides in aqueous alkaline solutions were investigated. The investigation revealed that each complex form only 1:1 (complex/carbohydrate molar ratio) species, even in the presence of stoichiometric excess of the carbohydrate in solution. Furthermore, the binding of D-mannose to each of the complexes were determined to be stronger than D-xylose, D-glucose, or xylitol.

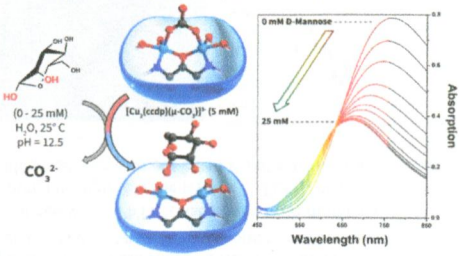

10989 dx.doi.org/10.1021/ic501390r

Structure and Magnetic Properties of the Spin-1/2-Based Honeycomb $NaNi_2BiO_{6-\delta}$ and Its Hydrate $NaNi_2BiO_{6-\delta}\cdot 1.7H_2O$

Elizabeth M. Seibel,* John H. Roudebush, Mazhar N. Ali, K. A. Ross, and R. J. Cava

The synthesis of the honeycomb compounds $NaNi_2BiO_{6-\delta}$ and its hydrate $NaNi_2BiO_{6-\delta}\cdot 1.7H_2O$ are reported. We investigate the structure and magnetic properties of these spin-1/2-based compounds. The hydrated honeycomb $NaNi_2BiO_{6-\delta}\cdot 1.7H_2O$ is a quasi-2-D magnetic system.

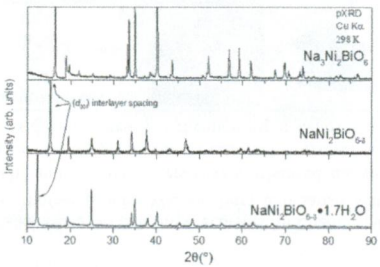

10996 dx.doi.org/10.1021/ic501431c

Spontaneous Redox Synthesis and Characterization of the Tetrathiafulvalene–Vanadium-Substituted Polyoxometalate Charge-Transfer Material $TTF_4[SVW_{11}O_{40}]$: Comparison with the Mo Analogue

Qi Li, Jinzhen Lu, John F. Boas, Daouda A. K. Traore, Matthew C. J. Wilce, Lisandra L. Martin, Tadaharu Ueda,* and Alan M. Bond*

The TTF radical cation–polyoxometalate salt $TTF_4[SVW_{11}O_{40}]$ has been prepared via spontaneous redox synthesis. Evidence based on a single-crystal X-ray structural analysis of $TTF_4[SVW_{11}O_{40}]\cdot 2H_2O\cdot 2CH_2Cl_2$ and data from Raman spectra imply that the two crystallographically distinguishable $(TTF)_2^{2+}$ dimers present in the structure have an asymmetric charge distribution. This is in contrast to the Mo analogue, where only symmetric $(TTF^{1+}\text{-}TTF^{1+})$ dimers are present. The unusual charge distribution is reflected in conductivity and the EPR data.

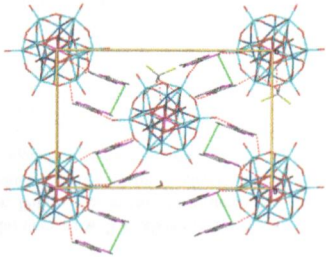

11007 dx.doi.org/10.1021/ic501423p

$Ba_{1.3}Ca_{0.7}SiO_4:Eu^{2+},Mn^{2+}$: A Promising Single-Phase, Color-Tunable Phosphor for Near-Ultraviolet White-Light-Emitting Diodes

Wenzhen Lv, Mengmeng Jiao, Qi Zhao, Baiqi Shao, Wei Lü, and Hongpeng You*

Newly synthesized $Ba_{1.3}Ca_{0.7}SiO_4:Eu^{2+},Mn^{2+}$ phosphors whose luminescent color can be easily adjusted from blue to red with variation of Mn^{2+} contents show great potential application for UV-LEDs.

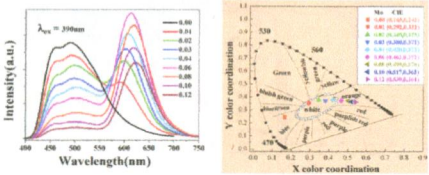

11015 dx.doi.org/10.1021/ic501430x

Exploring the Triplet Excited State Potential Energy Surfaces of a Cyclometalated Pt(II) Complex: Is There Non-Kasha Emissive Behavior?

Daniel Escudero* and Walter Thiel

The complexity of the emissive processes in a cyclometalated Pt(II) complex is demonstrated. The computational evidence points to non-Kasha emissive behavior at long time scales. Both the radiative and nonradiative deactivation mechanisms have been unraveled for this complex.

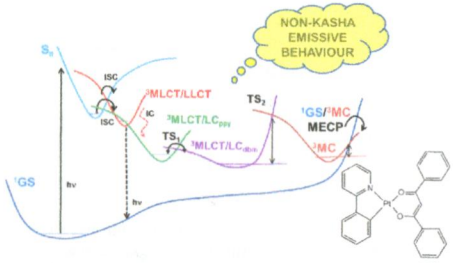

11020 S dx.doi.org/10.1021/ic501519a

Theoretical Modeling of Spin Crossover in Metal–Organic Frameworks: $[Fe(pz)_2Pt(CN)_4]$ as a Case Study

Jordi Cirera, Volodymyr Babin, and Francesco Paesani*

Using ab initio parametrized LF FFs that correctly reproduce the relative energies between the different spin-states for the secondary building units of the $[Fe(pz)_2Pt(CN)_4]$ MOF, a hybrid MC/MD approach is developed and used to determine the equilibrium populations of both LS and HS states of the material as a function of temperature, which allows calculation of the transition temperature. The calculated magnetic susceptibility curve for the MOF material agrees well with corresponding experimental values.

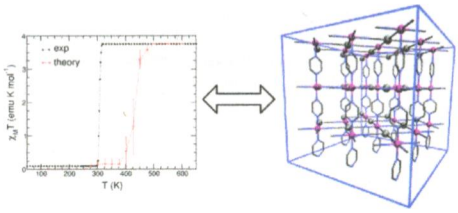

11029 S dx.doi.org/10.1021/ic501531g

Iron(II) Complexes Supported by Sulfonamido Tripodal Ligands: Endogenous versus Exogenous Substrate Oxidation

Sarah A. Cook, Joseph W. Ziller, and A. S. Borovik*

Oxidation of an Fe(II) complex supported by a sulfonamido tripodal ligand was explored with dioxygen and an O-atom transfer reagent. While dioxygen gave an Fe(III)–hydroxido complex, the O-atom transfer reagent resulted in C–H activation of the ligand to form an Fe(III)–alkoxide species. Modification of the ligand prevented this ligand oxidation and allowed for activation of C–H bonds on an external substrate.

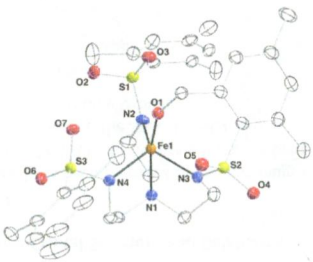

11036 S dx.doi.org/10.1021/ic501553m

Lattice Solvent and Crystal Phase Effects on the Vibrational Spectra of $UO_2Cl_4^{2-}$

David D. Schnaars and Richard E. Wilson*

The Raman and FT-IR spectra of a series of $UO_2Cl_4^{2-}$ polymorphs were collected and studied as functions of crystallographic phase and cocrystallized solvent. The data demonstrate the sensitivity of the uranyl(VI) vibrational frequencies to chemical environments beyond the first coordination sphere and highlight the need to understand the chemical structure of such materials before drawing chemical conclusions based on the vibrational spectra alone.

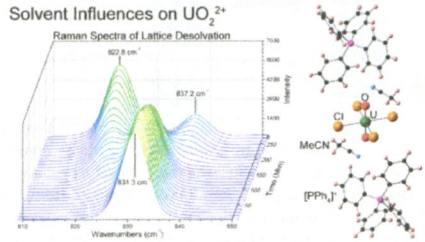

11046 S dx.doi.org/10.1021/ic501567s

Anion-Induced Supramolecular Isomerism in Two Preyssler P_5W_{30} Polyoxometalate-Based Hybrid Materials

Ya-Qin Zhao, Kai Yu, Li-Wei Wang, Ying Wang, Xing-Po Wang, and Di Sun*

Two extended Preyssler P_5W_{30} polyoxometalate-based inorganic−organic hybrid materials exhibiting anion-induced supramolecular isomerism were reported. Because of the *cis*−*trans* isomerism in the octahedral CoN_2O_4 coordination geometry, the Preyssler P_5W_{30} polyoxometalates are extended by double O−Co−O bridges in **1*α*** and a single O−Co−O bridge in **1*β*** to form the isomeric 2D 4-connected 4^4-**sql** and 3D 8-connected **bcu** networks, respectively. Both compounds show electrocatalytic abilities on the reduction of H_2O_2.

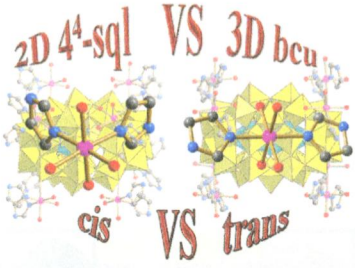

11051 S dx.doi.org/10.1021/ic501569e

Multiporphyrin Arrays on Cyclotriphosphazene Scaffolds

Tejinder Kaur, Malakalapalli Rajeswararao, and Mangalampalli Ravikanth*

Hexaporphyrin and dodecaporphyrin assemblies on cyclotriphosphazene scaffolds were synthesized in decent yields under simple reaction conditions, and their molecular structures were elucidated using 1D and 2D NMR spectroscopy.

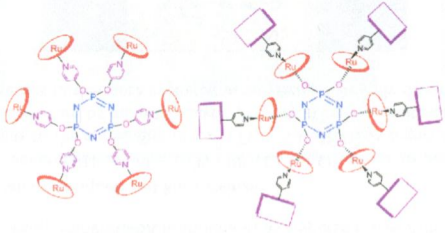

11060 dx.doi.org/10.1021/ic501604c

Formation Mechanism of (001) Oriented Perovskite $SrTiO_3$ Microplatelets Synthesized by Topochemical Microcrystal Conversion

Yunfei Chang,* Huanpo Ning, Jie Wu, Shantao Zhang, Tianquan Lü, Bin Yang,* and Wenwu Cao

(001) oriented perovskite $SrTiO_3$ microplatelets with a controlled morphology (~5 μm in length and ~0.4 μm in thickness) were synthesized by topochemical microcrystal conversion (TMC) from Aurivillius $SrBi_4Ti_4O_{15}$ platelike precursors. Compositional/structural evolutions, morphological development, and reaction interface evolution during the Aurivillius $SrBi_4Ti_4O_{15}$ to perovskite $SrTiO_3$ conversion process was investigated by X-ray diffraction, Raman scattering, differential thermal analysis, field-emission scanning electron microscopy, and transmission electron microscopy measurements. The possible TMC mechanism was interpreted.

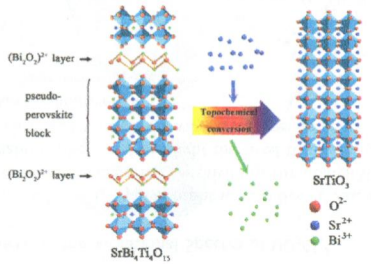

11068 S dx.doi.org/10.1021/ic5015797

Ligand-Controlled Syntheses of Copper(I) Complexes with Metal–Metal Interactions: Crystal Structure and Relativistic Density Functional Theory Investigation

Jun-Feng Liu, Xue Min, Jin-Yu Lv, Fu-Xing Pan, Qing-Jiang Pan,* and Zhong-Ming Sun*

A family of di-, tri-, and tetranuclear copper(I) complexes with metal–metal interactions have been prepared by rational length control of silaamidinate ligands. These complexes show short Cu^I–Cu^I distances (2.43–2.62 Å) and feature a linear or bent metal–metal arrangement. The relativistic density functional theory calculations have rationalized the short Cu–Cu distances by the metal–metal attractive interaction that comes from the strong and stable σ- and π-bonding orbitals.

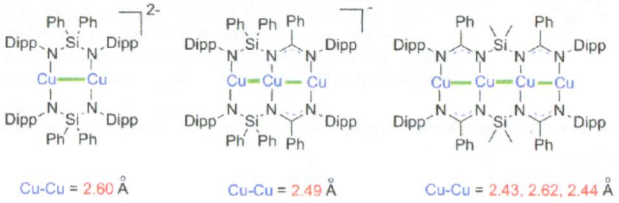

11075 $

dx.doi.org/10.1021/ic501620g

Photoinduced Electron Transfer in Rhenium(I)–Oligotriarylamine Molecules

Annabell G. Bonn, Markus Neuburger, and Oliver S. Wenger*

The possibility of accumulating two positive charges on oligotriarylamine units after photoexcitation of purely molecular systems in CH_3CN was explored by transient absorption spectroscopy. The rhenium(I) tricarbonyl diimine photosensitizers employed in this study turned out to be a suboptimal choice for this purpose, and it is concluded that future research in this direction will benefit from the use of robust photosensitizers, which absorb at longer wavelengths.

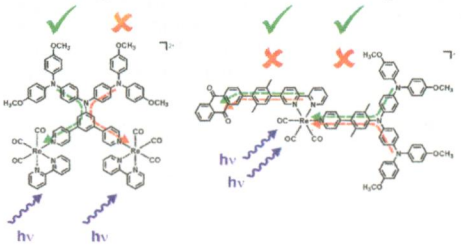

11086 $

dx.doi.org/10.1021/ic501644z

Dual Application of (Aqua)(Chlorido)(Porphyrinato)Chromium(III) as Hypersensitive Amine-Triggered ON Switch and for Dioxygen Activation

Philip Heier, Nicolas D. Boscher, Patrick Choquet, and Katja Heinze*

The tetraphenyl porphyrinato chromium(III) complex $Cr^{III}(TPP)(Cl)(H_2O)$ shows an unexpected dichotomous reactivity toward amines. This reactivity leads to the application of $Cr^{III}(TPP)(Cl)(H_2O)$ as highly sensitive substoichiometric and irreversible ON switch for amine detection by an autocatalytic pathway. The concomitant activation of O_2 by the $Cr^{III}(TPP)(Cl)(H_2O)$/amine system is furthermore exploited in an electrochemically driven epoxidation of norbonene using O_2 as initial oxidant.

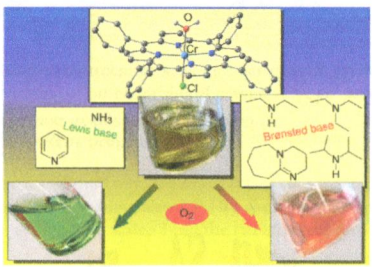

11096 S dx.doi.org/10.1021/ic5016675

Models for B_{12}-Conjugated Radiopharmaceuticals. Cobaloxime Binding to New *fac*-[Re(CO)$_3$(Me$_2$Bipyridine)(amidine)]BF$_4$ Complexes Having an Exposed Pyridyl Nitrogen

Nerissa A. Lewis, Patricia A. Marzilli, Frank R. Fronczek, and Luigi G. Marzilli*

The cyclic C_2-symmetrical amine 1-(4-pyridyl)piperazine readily reacts with *fac*-[Re^I(CO)$_3$(Me$_2$bipy)(CH$_3$CN)]BF$_4$ to form new amidine complexes *fac*-[Re(CO)$_3$(Me$_2$bipy)(HNC(CH$_3$)(pyppz))]BF$_4$. Such amidine complexes have an exposed, highly basic pyridyl nitrogen that readily coordinates to the cobalt atom in a simple B_{12} model, (py)Co(DH)$_2$Cl (DH = monoanion of dimethylglyoxime), producing dinuclear *fac*-[Re(CO)$_3$(Me$_2$bipy)(μ-(HNC(CH$_3$)(pyppz)))Co(DH)$_2$Cl]BF$_4$ complexes. The successful conjugation of the *fac*-[Re^I(CO)$_3$] core to a B_{12} model provides guidance for the development of ^{99m}Tc and $^{186/188}$Re radiopharmaceuticals for targeted tumor imaging and therapy.

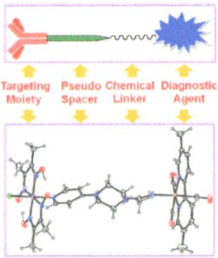

11108 S dx.doi.org/10.1021/ic501683t

DNA-Binding Studies of a Tetraalkyl-Substituted Porphyrin and the Mutually Adaptive Distortion Principle

Srijana Ghimire, Phillip E. Fanwick, and David R. McMillin*

Results from circular dichroism, absorbance, and emission spectroscopies, as well as viscometry and X-ray crystallography, reveal the DNA-binding interactions of various forms of the alkyl-substituted cationic porphyrin H_2TC3. These ligands may be useful for photodynamic and/or anticancer therapy. Interestingly, H_2TC3 and Cu(TC3) interact differently with a ds DNA host that is rich in adenine-thymine base pairs. Intercalation is the exclusive binding motif found for the comparatively rigid form Cu(TC3), but external binding is a competitive process with H_2TC3.

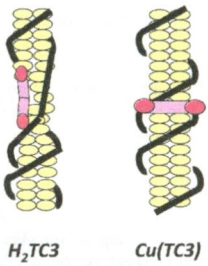

11119 S dx.doi.org/10.1021/ic501679f

Cation Substitution Dependent Bimodal Photoluminescence in Whitlockite Structural $Ca_{3-x}Sr_x(PO_4)_2$:Eu^{2+} ($0 \le x \le 2$) Solid Solution Phosphors

Haipeng Ji, Zhaohui Huang,* Zhiguo Xia,* Maxim S. Molokeev, Victor V. Atuchin, and Saifang Huang

Cation substitution dependent tunable bimodal photoluminescence is observed in the $Ca_{3-x}Sr_x(PO_4)_2$:Eu^{2+} ($0 \le x \le 2$) solid solution phosphors. In addition to the emission band peak at 416 nm in $Ca_3(PO_4)_2$:Eu^{2+}, the substitution of Ca^{2+} by Sr^{2+} induces an emerging band peak at 493 nm. This interesting bimodal photoluminescence originates from the EuO_n−Ca_9 and EuO_n−$Ca_{9-y}Sr_y$ emitting blocks, respectively.

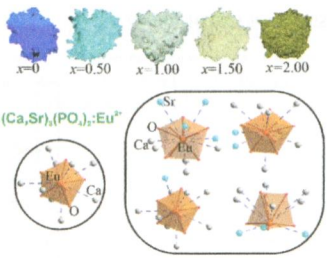

11125 S dx.doi.org/10.1021/ic501687h

Design and Synthesis of a New Layered Thermoelectric Material $LaPbBiS_3O$

Yun-Lei Sun, Abduweli Ablimit, Hui-Fei Zhai, Jin-Ke Bao, Zhang-Tu Tang, Xin-Bo Wang, Nan-Lin Wang, Chun-Mu Feng, and Guang-Han Cao*

A new quinary oxysulfide $LaPbBiS_3O$ is composed of stacked NaCl-like $[M_4S_6]$ (M = Pb, Bi) layers and fluorite-type $[La_2O_2]$ layers. The thermopower and the figure of merit at room temperature were measured to be −52 μV/K and 0.23, respectively.

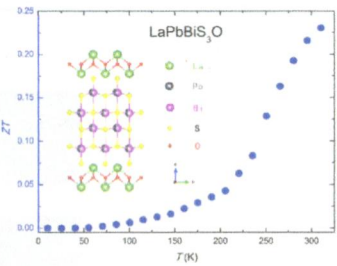

11130 S dx.doi.org/10.1021/ic501710k

Osmium(III) Analogues of KP1019: Electrochemical and Chemical Synthesis, Spectroscopic Characterization, X-ray Crystallography, Hydrolytic Stability, and Antiproliferative Activity

Paul-Steffen Kuhn, Gabriel E. Büchel, Katarina K. Jovanović, Lana Filipović, Siniša Radulović, Peter Rapta, and Vladimir B. Arion*

Osmium(III) analogues of the lead investigational anticancer drug KP1019 were prepared by one-electron reduction of previously reported osmium(IV) complexes *trans*-$[OsCl_4(Hazole)_2]$, where Hazole = 1*H*-pyrazole, 2*H*-indazole, 1*H*-imidazole, and 1*H*-benzimidazole. Their crystal structures, spectroscopic properties, hydrolytic stability, and reactivities toward amino acids and 5′-dGMP, as well as antiproliferative activities in human cancerous and noncancerous cell lines, were studied.

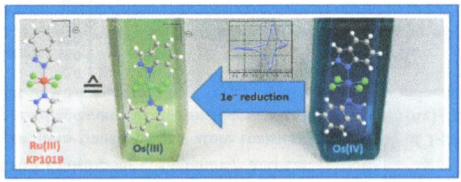

11140 S dx.doi.org/10.1021/ic501747e

Neutron Diffraction Studies of a Four-Coordinated Hydride in Near Square-Planar Geometry

Jian-Hong Liao, Rajendra Singh Dhayal, Xiaoping Wang, Samia Kahlal, Jean-Yves Saillard, and C. W. Liu*

The structure of a nanospheric polyhydrido copper cluster, $[Cu_{20}(H)_{11}\{S_2P(O^iPr)_2\}_9]$, was determined by single-crystal neutron diffraction. The 11 hydrides in the cluster display three different coordination modes to the Cu atoms: six μ_3-hydrides in a pyramidal geometry, two μ_4-hydrides in a tetrahedral cavity, and three μ_4-hydrides in an unprecedented near square-planar geometry.

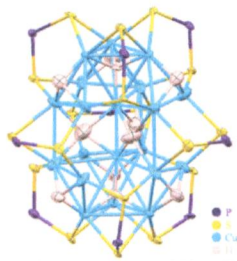

11146 S dx.doi.org/10.1021/ic501749c

Temperature-Triggered Reversible Dielectric and Nonlinear Optical Switch Based on the One-Dimensional Organic–Inorganic Hybrid Phase Transition Compound $[C_6H_{11}NH_3]_2CdCl_4$

Wei-Qiang Liao, Heng-Yun Ye, Da-Wei Fu, Peng-Fei Li, Li-Zhuang Chen, and Yi Zhang*

The one-dimensional organic–inorganic hybrid compound bis(cyclohexylammonium) tetrachlorocadmate(II) exhibits two structural phase transitions, at 215 and 367 K. In addition, both the dielectric constant and second harmonic generation intensity of this compound show a striking change between low and high states at around 367 K.

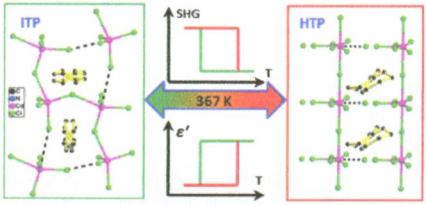

11152 S dx.doi.org/10.1021/ic5017565

Interactions of Octahedral Ruthenium(II) Polypyridyl Complexes with the RNA Triplex poly(U)•poly(A)*poly(U) Effect on the Third-Strand Stabilization

Xiao-Jun He and Li-Feng Tan*

Stable triplexes play key roles in many biological processes. Due to the Hoogsteen base pairing, triplexes are, however, thermodynamically less stable than the corresponding duplexes. The poor stabilization of these structures limits their practical applications under physiological conditions. To understand the effect of the factors on the stabilization of RNA triplexes by octahedral ruthenium(II) complexes, the interactions of Ru**1** and Ru**2** with the RNA triplex poly(U)•poly(A)*poly(U) are examined in this work. The main results obtained here suggest that the third-strand stabilization depends on the hydrophobicity effects of ancillary ligands bpy and phen.

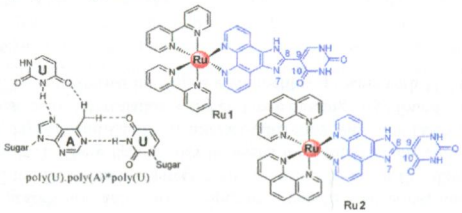

11160 S dx.doi.org/10.1021/ic5017033

Activation of Nitrogen Brønsted Acids: Synthesis and Reactivity of a New Class of Nitrogen Acid Complexes

D. Scott Bohle* and Zhijie Chua

The addition of nitrogen acids to Ir(I) leads to new ligands with unusual O-bound nitro groups.

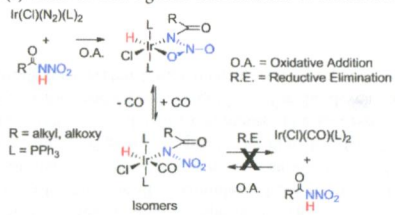

11173 dx.doi.org/10.1021/ic5017615

Two New Arsenides, $Eu_7Cu_{44}As_{23}$ and $Sr_7Cu_{44}As_{23}$, With a New Filled Variety of the $BaHg_{11}$ Structure

Dmitri O. Charkin, Roman Demchyna, Yurii Prots, Horst Borrmann, Ulrich Burkhardt, Ulrich Schwarz, Walter Schnelle, Igor V. Plokhikh, Sergey M. Kazakov, Artem M. Abakumov, Dmitry Batuk, Valery Yu. Verchenko, Alexander A. Tsirlin, Caroline Curfs, Yuri Grin,* and Andrei V. Shevelkov*

The crystal structure of $A_7Cu_{44}As_{23}$ (A = Eu, Sr) can be described as a set of five shells, or nested polyhedra, around the A^{2+} cation (see Figure). The resulting framework of copper and arsenic atoms features clathrate-like voids filled by Eu(Sr) and As atoms in an ordered fashion. Although the compounds are metals, they exhibit very low thermal conductivity; ferromagnetic ordering is observed at 17.5 K for the Eu derivative.

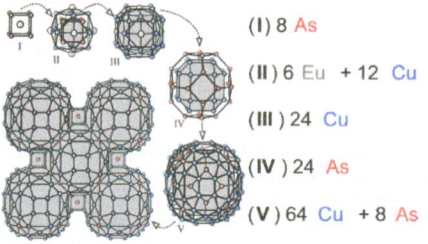

11185 dx.doi.org/10.1021/ic5017005

Role of Axial Base Coordination in Isonitrile Binding and Chalcogen Atom Transfer to Vanadium(III) Complexes

Subhojit Majumdar, Julia M. Stauber, Taryn D. Palluccio, Xiaochen Cai, Alexandra Velian, Elena V. Rybak-Akimova,* Manuel Temprado,* Burjor Captain,* Christopher C. Cummins,* and Carl D. Hoff*

Thermochemical studies of oxygen atom transfer, sulfur atom transfer, and binding of 1-adamantyl isocyanide to $V[(Me_3SiNCH_2CH_2)_3N]$ are reported and compared to analogous data for $V(N[t\text{-}Bu]Ar)_3$, **2**, (Ar = 3,5-$C_6H_3Me_2$). Reactions of $V[(Me_3SiNCH_2CH_2)_3N]$ result in weakening of the V–N_{axial} bond and directly influence reaction energetics.

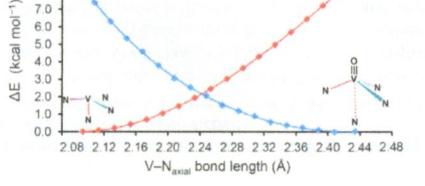

11197 S dx.doi.org/10.1021/ic5017802

P2-$Na_xMn_{1/2}Fe_{1/2}O_2$ Phase Used as Positive Electrode in Na Batteries: Structural Changes Induced by the Electrochemical (De)intercalation Process

Benoit Mortemard de Boisse, Dany Carlier,* Marie Guignard, Lydie Bourgeois, and Claude Delmas

The structural transitions accompanying the sodium (de)intercalation in the $Na_xMn_{1/2}Fe_{1/2}O_2$ system have been studied by operando in situ X-ray powder diffraction. The P′2 structure of the intercalated phase was confirmed by synchrotron X-ray powder diffraction. The present work also gives an insight into the structural mechanisms the material undergoes in the 4.0−4.3 V vs Na^+/Na voltage region.

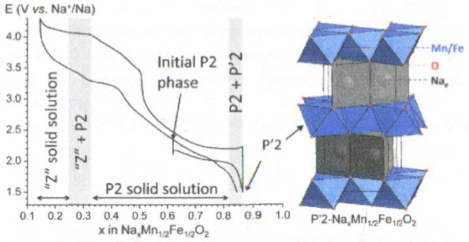

11206 S dx.doi.org/10.1021/ic501801f

Synthesis of Two Triarylboron-Functionalized Metal−Organic Frameworks: In Situ Decarboxylic Reaction, Structure, Photoluminescence, and Gas Adsorption Properties

Xiaoqing Wang, Jie Yang, Liangliang Zhang, Fuling Liu, Fangna Dai,* and Daofeng Sun*

Two triarylboron-functionalized MOFs (**1** and **2**) with different topologies have been synthesized on the basis of a trigonal carboxylate ligand, and the decarboxylation is observed in the preparation of **2**. Due to the different stability of the SBU in **1** and **2**, they show different gas uptakes, which have been fully studied for complex **2**.

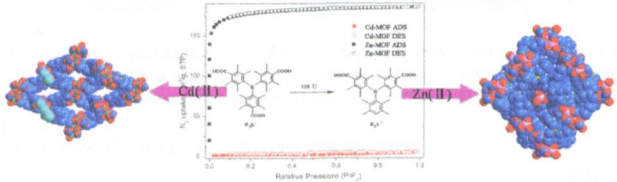

11213 S dx.doi.org/10.1021/ic501814q

Effect of Halogen (Cl, Br) on the Symmetry of Flexible Perovskite-Related Framework

Chunyan Bai, Hongwei Yu, Shujuan Han,* Shilie Pan,* Bingbing Zhang, Ying Wang, Hongping Wu, and Zhihua Yang*

All three crystals of $Na_3B_6O_{10}Cl$, $RbNa_2B_6O_{10}Cl$, and $RbNa_2B_6O_{10}Br$ exhibit an intricate 3D network, which are built up by B_6O_{13} groups and six coordinated XM_6 (X = Cl, Br; M = Na, Rb) polyhedra. The structure of them can be described as the B_6O_{13} network and XM_6 (X = Cl, Br; M = Na, Rb) network interweaved to form an intricate 3D network.

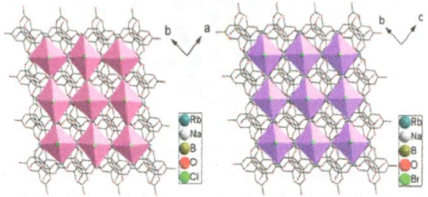

11221 Ⓢ dx.doi.org/10.1021/ic501788v

Inhibitory Act of Selenoprotein P on Cu^{+}/Cu^{2+}-Induced Tau Aggregation and Neurotoxicity

Xiubo Du, Youbiao Zheng, Zhi Wang, Yijing Chen, Rui Zhou, Guoli Song, Jiazuan Ni,* and Qiong Liu*

Alzheimer's disease tau peptide binds 0.44 Cu^{2+} and 0.34 Cu^{+} per monomer with dissociation constants of 1.1 nM and 0.2 pM, respectively. Cu^{+} and Cu^{2+} stimulated aggregation, ROS production, and neuronal cytotoxicity of tau peptide. More intriguingly, copper-associated tau aggregates decreased protein levels of MAP-2 and synaptophysin in neurons and reduced mitochondrial density and mobility in the axon. All these effects of copper were significantly restored by the His-rich domain of selenoprotein P.

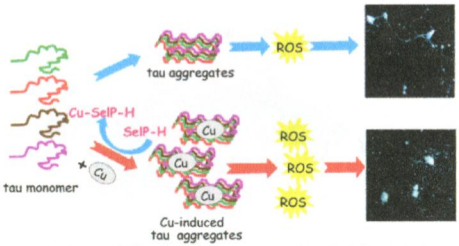

11231 Ⓢ dx.doi.org/10.1021/ic5018246

Morphotropy and Temperature-Driven Polymorphism in $A_2Th(AsO_4)_2$ (A = Li, Na, K, Rb, Cs) Series

Na Yu, Vladislav V. Klepov, Giuseppe Modolo, Dirk Bosbach, Evgeny V. Suleimanov, Thorsten M. Gesing, Lars Robben, and Evgeny V. Alekseev*

A novel family of Th-based phases with $A_2Th(AsO_4)_2$ (A = Li, Na, K, Rb, Cs) composition was synthesized and systematically investigated. Morphotropic transition with significant structural changes was observed in the series. Coordination geometry of Th centers changes from Li to Cs in studied compounds. High-temperature displacive phase transitions have been observed in the structures of K and Rb members.

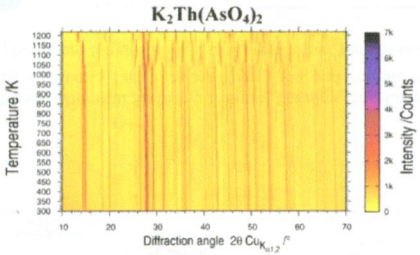

11242 S dx.doi.org/10.1021/ic501840p

Dinuclear Rhenium Complexes as Redox-Active Pendants in a Novel Electrodeposited Polycyclopentadithiophene Material

Elsa Quartapelle Procopio, Valentina Bonometti, Monica Panigati,* Pierluigi Mercandelli,* Patrizia R. Mussini,* Tiziana Benincori, Giuseppe D'Alfonso, and Francesco Sannicolò

A new dinuclear hydridocarbonylrhenium complex bearing a pyridazine ligand and a coordinated cyclopentadithiophene moiety has been prepared and oxidatively electropolymerized, affording an electroactive thiophene-based polymer regularly decorated with the rhenium complexes. Detailed spectroscopic and electrochemical characterization indicated that it behaves as a metallo-polymer, in which the conductive properties of the π-conjugated system are added to the redox behavior of the pendant-isolated complexes.

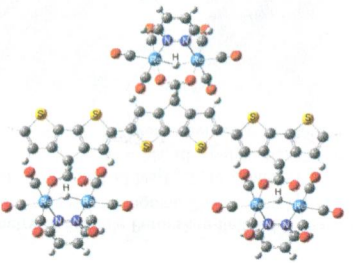

11252 S dx.doi.org/10.1021/ic501841e

Aqueous Hafnium Sulfate Chemistry: Structures of Crystalline Precipitates

Ali Kalaji and L. Soderholm*

Single crystals were isolated and structures obtained from a series of Hf solutions with varying pH and sulfate concentrations. The systematic changes in cluster size with increasing pH and decreasing sulfate concentration reveal the differing roles of hydrolysis, which increases the size of Hf oxyhydroxo oligomers, and the sulfate anion, which acts to cap the cluster surface, thereby limiting cluster size.

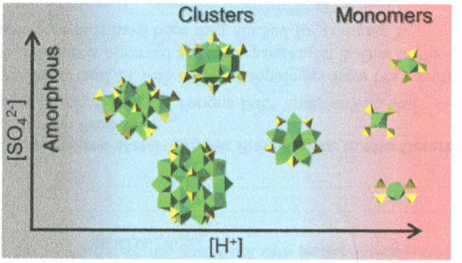

11261 S dx.doi.org/10.1021/ic501857f

Mild P–P Bond Cleavage in the Methyldiphosphenyl Complex $[Mo_2Cp_2(\mu\text{-}PCy_2)(\mu\text{-}\kappa^2\kappa^2\text{-}P_2Me)(CO)_2]$ To Give Novel Phosphide-Bridged Trinuclear Derivatives

M. Angeles Alvarez, M. Esther García, Daniel García-Vivó, Raquel Lozano, Alberto Ramos,* and Miguel A. Ruiz*

Room-temperature reactions of the title complex with suitable precursors of carbonylic ML_n fragments (M = Mo, W, Fe) eventually result in P–P bond cleavage processes in the diphosphenyl ligand, to give trinuclear derivatives bridged by pyramidal phosphide and phosphinidene ligands or by a trigonal-planar phosphide ligand.

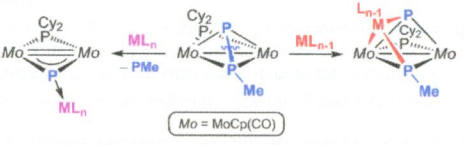

11274 S dx.doi.org/10.1021/ic501865h

Derivation of Structure–Activity Relationships from the Anticancer Properties of Ruthenium(II) Arene Complexes with 2-Aryldiazole Ligands

Marta Martínez-Alonso, Natalia Busto, Félix A. Jalón, Blanca R. Manzano, José M. Leal, Ana M. Rodríguez, Begoña García,* and Gustavo Espino*

The cytototoxic activity of new ruthenium(II) arene compounds with 2-aryldiazole ligands has been evaluated in several cell lines (MCR-5, MCF-7, A2780, and A2780cis) in order to establish structure–activity relationships. Moreover, DNA binding measurements for three of the compounds differing in the arene moiety have been carried out. All of them can interact with DNA. Nevertheless, while the derivative with *p*-cymene strongly destabilizes DNA, those with benzene and 2-phenoxyethanol have little effect on the DNA double helix stability.

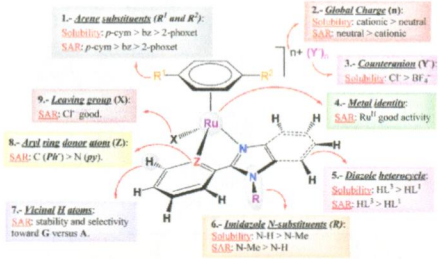

11289 S dx.doi.org/10.1021/ic501923s

Lithium Silicide Nanocrystals: Synthesis, Chemical Stability, Thermal Stability, and Carbon Encapsulation

Jacqueline E. Cloud, Yonglong Wang, Xuemin Li, Tara S. Yoder, Yuan Yang, and Yongan Yang*

A systematic study of synthesizing phase-pure lithium silicide nanocrystals and the physicochemical properties of two model systems are presented.

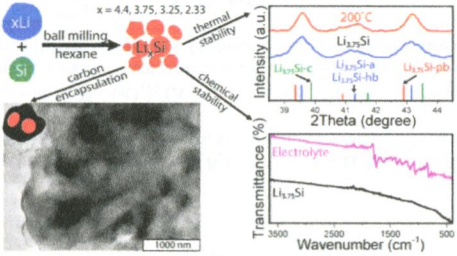

11298 S dx.doi.org/10.1021/ic501889u

Photoinduced Mixed Valency in Zinc Porphyrin Dimer of Triruthenium Cluster Dyads

Jane Henderson and Clifford P. Kubiak*

A strongly coupled mixed-valence state following an photodriven intramolecular electron transfer from an excited zinc porphyrin to a Ru_3O dimer was observed in systems of the form $(ZnTPPpy)Ru_3O(OAc)_6(CO)$-pz-$Ru_3O(OAc)_6(CO)L$, where ZnTPPpy = zinc(II) 5-(4-pyridyl)-10,15,20-triphenylporphyin, L = pyridyl ligand, and pz = pyrazine. The ground-state characterization of these stable, singly reduced species allowed for confirmation of a photoinduced mixed-valence state, and the corresponding strong electronic coupling is explored.

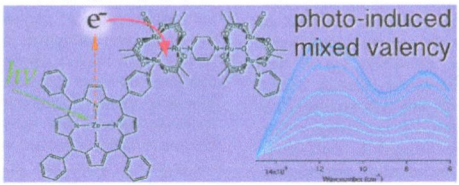

11307 S dx.doi.org/10.1021/ic5019778

Synthesis and Characterization of Heterobimetallic Complexes with Direct Cu–M Bonds (M = Cr, Mn, Co, Mo, Ru, W) Supported by *N*-Heterocyclic Carbene Ligands: A Toolkit for Catalytic Reaction Discovery

Suparna Banerjee, Malkanthi K. Karunananda, Sharareh Bagherzadeh, Upul Jayarathne, Sean R. Parmelee, Greyson W. Waldhart, and Neal P. Mankad*

A toolbox of heterobimetallic complexes featuring (NHC)Cu fragments with fine-tuning of steric and electronic parameters was constructed and thoroughly characterized.

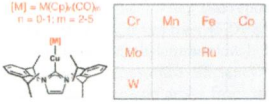

11316 S dx.doi.org/10.1021/ic5019967

Near-Infrared Electrochromism in Electropolymerized Metallopolymeric Films of a Phen-1,4-diyl-Bridged Diruthenium Complex

Hai-Jing Nie and Yu-Wu Zhong*

Reductive electropolymerization of the phen-1,4-diyl-bridged diruthenium complex with four vinyl substituents afforded adhesive metallopolymeric films on platinum and ITO glass electrode surfaces, which display promising electrochromism at the fiber-optic communication wavelength (1300 nm) with a good contrast ratio and low operation potential.

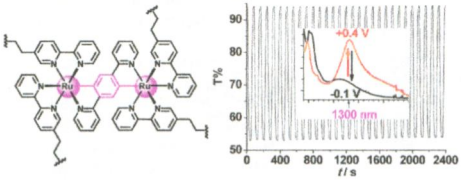

11323 (S) dx.doi.org/10.1021/ic5020253

Molecular Anisotropy Analysis of Single-Ion Magnets Using an Effective Electrostatic Model

José J. Baldoví, Juan M. Clemente-Juan, Eugenio Coronado,* and Alejandro Gaita-Ariño*

The lone pair effective charge model is used to reproduce the angular dependence of the magnetic susceptibility in single crystals of pentamethylcyclopentadienyl-Er-cyclooctatetraene single-ion magnet. The π-cloud displacement is essential to describe the magnetic anisotropy in aromatic ligands. Furthermore, the parametrization of the ligands obtained in this study has been extrapolated to reproduce spectroscopic data of mononuclear lanthanoid complexes based on the same kind of ligands, emphasizing the predictive character of this model.

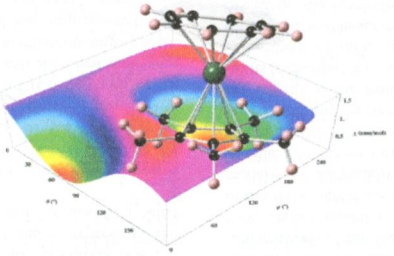

11328 (S) dx.doi.org/10.1021/ic502108a

Cooperative Effects of Cation Size and Variable Coordination Modes of Te^{4+} on the Frameworks of New Alkali Metal Indium Tellurites, $NaIn(TeO_3)_2$, $KIn(TeO_3)_2$, $RbInTe_3O_8$, and $CsInTe_3O_8$

Su-whan Bae, Choong-Yeol Kim, Dong Woo Lee, and Kang Min Ok*

Four new alkali metal indium tellurites, $NaIn(TeO_3)_2$, $KIn(TeO_3)_2$, $RbInTe_3O_8$, and $CsInTe_3O_8$ have been synthesized through solid state and hydrothermal reactions. The size of the alkali metal cations and variable coordination modes of Te^{4+} cations cooperatively influence the framework geometries of the mixed metal tellurites.

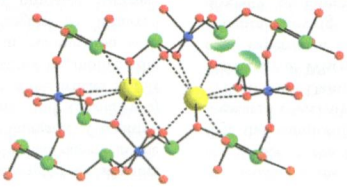

11335 S dx.doi.org/10.1021/ic5022164

Metal–Ligand Cooperation in H_2 Activation with Iron Complexes Bearing Hemilabile Bis(diphenylphosphino)amine Ligands

Nicolas Frank, Katharina Hanau, and Robert Langer*

By means of variable-temperature ^{1}H-EXSY NMR spectroscopy, the small-bite-angle diphosphine ligand bis-(diphenylphosphino)amine is shown to be hemilabile in an octahedral iron(II) complex. As the deprotonated ligand can act as an internal base, the reversible generation of a vacant coordination site allows for dihydrogen coordination and heterolytic cleavage.

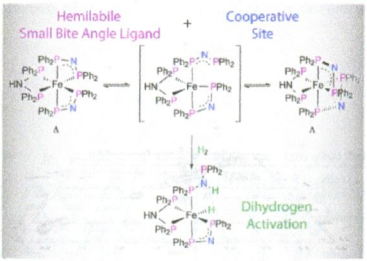

S Supporting Information available via online article